

FROM MUTATION TO DEGRADATION: PREDICTING NONSENSE-MEDIATED DECAY WITH NMDEP

Ali Saadat, Jacques Fellay

School of Life Sciences

Ecole Polytechnique Fédérale de Lausanne

Lausanne, Switzerland

{ali.saadat, jacques.fellay}@epfl.ch

ABSTRACT

Nonsense-mediated mRNA decay (NMD) is a critical post-transcriptional surveillance mechanism that degrades transcripts with premature termination codons, safeguarding transcriptome integrity and shaping disease phenotypes. However, accurately predicting NMD efficiency remains challenging, as existing models often rely on simplistic rule-based heuristics or limited feature sets, constraining their accuracy and generalizability. Using paired DNA and RNA data from The Cancer Genome Atlas, we benchmark embedding-only models and demonstrate that they underperform compared to a simple rule-based approach. To address this, we develop NMDEP (NMD Efficiency Predictor), an integrative framework that combines optimized rule-based methods, sequence embeddings, and curated biological features, achieving state-of-the-art predictive performance. Through explainable AI, we identify key NMD determinants, reaffirming established factors such as variant position while uncovering novel contributors like ribosome loading. Applied to over 2.9 million simulated stop-gain variants, NMDEP facilitates large-scale mRNA degradation assessments, advancing variant interpretation and disease research.

1 INTRODUCTION

Nonsense-mediated mRNA decay (NMD) is a crucial post-transcriptional regulatory mechanism that degrades mRNAs containing premature termination codons (PTCs) (Chang et al., 2007). By selectively eliminating erroneous transcripts, NMD plays a vital role in maintaining transcriptome integrity, regulating gene expression, and influencing disease phenotypes (Kurosaki et al., 2019). However, not all transcripts harboring PTCs undergo degradation, as some escape NMD due to context-dependent factors that modulate their stability (Figure 1). This variability complicates the computational prediction of NMD efficiency and its downstream effects on gene expression (Supek et al., 2021).

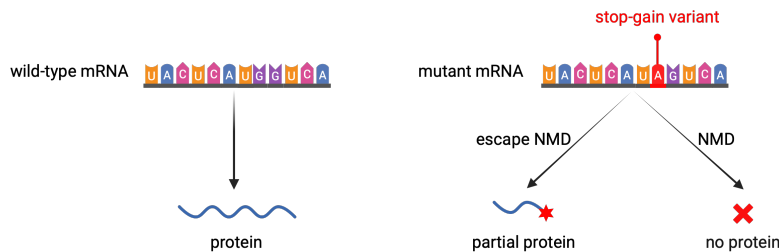


Figure 1: Left: A wild-type mRNA is translated into a full-length protein. Right: An mRNA containing a stop-gain variant can either undergo NMD, resulting in no protein production, or escape NMD, leading to the translation of a truncated protein. Figure created with BioRender.com.

Recent large-scale sequencing efforts, such as The Cancer Genome Atlas (TCGA) (Cancer Genome Atlas Research Network et al., 2013), have enabled the systematic analysis of NMD efficiency across diverse genetic backgrounds (Litchfield et al., 2020). In particular, allele-specific expression (ASE) patterns derived from paired DNA and RNA sequencing provide a means to quantify NMD efficiency at a single-variant resolution (Rivas et al., 2015).

Most existing methods have framed NMD efficiency prediction as a binary classification task (NMD vs. NMD escape), relying predominantly on rule-based heuristics (Lindeboom et al., 2016; Coban-Akdemir et al., 2018; Lindeboom et al., 2019; Klonowski et al., 2023; Torene et al., 2024) or limited feature sets (Teran et al., 2021; Kim et al., 2024), thereby restricting their accuracy and generalizability. Furthermore, these approaches often fail to account for context-dependent factors that modulate NMD efficiency. Consequently, there remains a critical need for more advanced models that incorporate rich sequence context and functional genomics data to enhance predictive performance.

To address these challenges, we explore the use of sequence embeddings from deep learning models trained on large-scale genomic data. We systematically evaluate multiple sequence aggregation strategies and compare embedding-based approaches with traditional feature-based models. Furthermore, we introduce NMDEP (NMD Efficiency Predictor), an integrative framework that combines optimized rule-based methods, deep-learning-derived embeddings, and curated biological features to achieve state-of-the-art predictive performance.

Our study benchmarks embedding-based methods for NMD efficiency prediction, showing that NMDEP outperforms rule-based and embedding-only models. Using explainable AI, we identify key NMD determinants, reaffirming known factors like variant position and uncovering novel contributors such as ribosome loading. Applying NMDEP to 2.9 million simulated stop-gain variants, we provide a large-scale resource for transcript stability assessments.

By integrating deep learning embeddings, curated biological features, and model interpretation, our framework advances NMD efficiency prediction, offering insights into transcriptome regulation and NMD escape mechanisms in disease.

2 METHODS

2.1 DATA COLLECTION

NMD efficiency The NMD efficiency dataset was obtained from Kim et al. (2024) which was constructed using paired DNA and RNA sequencing data from 9,235 samples in TCGA using 4,257 high-confidence nonsense variants. Since RNA-seq captures transcripts expressed in a cell, the variant allele frequency (VAF) observed in RNA sequencing (VAF_{RNA}) provides a measure of ASE, reflecting how much of a given allele’s transcript is retained after cellular regulatory processes, including NMD. In contrast, the VAF of the same variant observed in DNA sequencing (VAF_{DNA}) represents the allele frequency prior to transcript-level regulation, making it a suitable baseline estimate of VAF_{RNA} in the absence of NMD. To quantify NMD efficiency for each nonsense variant, the following equation was used: $NMD_{\text{efficiency}} = -\log_2 \left(\frac{VAF_{RNA}}{VAF_{DNA}} \right)$.

Data splitting We split the NMD efficiency dataset by chromosome to minimize the risk of information leakage. Chromosomes 20, 21, and 22 were assigned to the test set, chromosome 19 to the validation set, and the remaining chromosomes to the training set. This resulted in test, validation, and training splits of 5.5%, 5.1%, and 89.4%, respectively.

2.2 BENCHMARKING SEQUENCE EMBEDDING REPRESENTATIONS

Study design Since NMD efficiency prediction is a sequence-level phenotype influenced by a single nucleotide change, we conducted a systematic analysis to determine the optimal approach for predicting sequence-level outcomes from token embeddings. We evaluated three strategies: Aggregation First (AggFirst), Aggregation Last (AggLast), and a set neural network (DeepSet) (Zaheer et al., 2017). Token embeddings were generated for both reference (Ref) and alternative (Alt) mRNA sequences, and we explored two encoding strategies: using only Alt token embeddings or computing the difference between Alt and Ref embeddings (Alt – Ref). For each method, we tested four

aggregation functions including mean, max, sum, and token (i.e., using the token embedding at the variant position). Figure 2 provides an overview of our benchmarking study design.

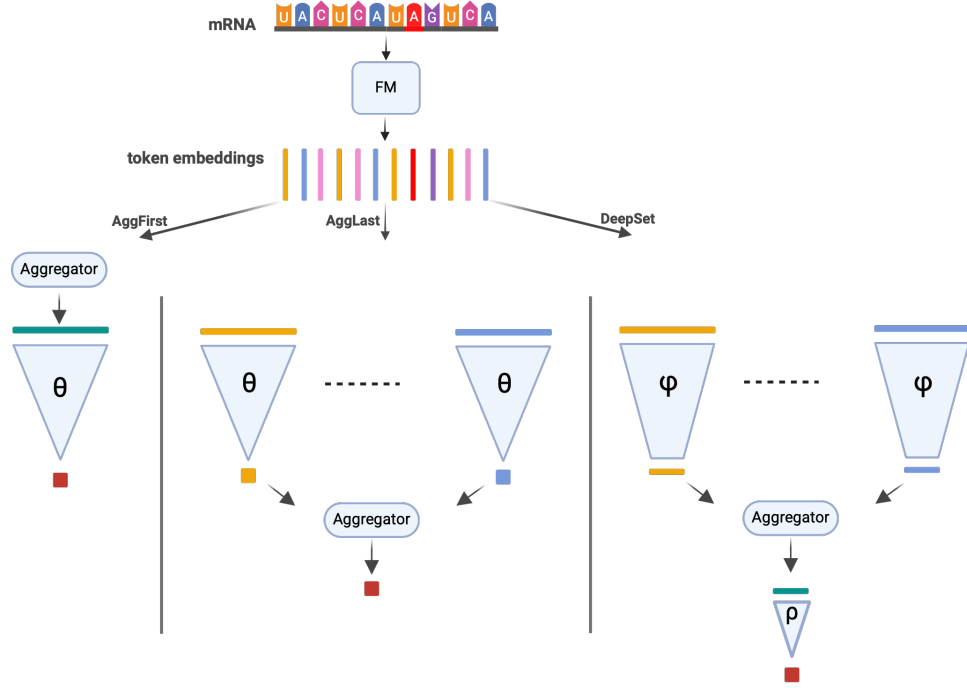


Figure 2: Evaluation of three strategies for embedding aggregation: Aggregation First (AggFirst), Aggregation Last (AggLast), and DeepSet. Token embeddings were generated for reference (Ref) and alternative (Alt) mRNA sequences, using either Alt embeddings alone or the difference (Alt – Ref). Four aggregation functions were tested: mean, max, sum, and token-level embedding. Figure created with BioRender.com

For formulation, we define \mathbf{A} as the aggregation function. Given an mRNA sequence of length L , each nucleotide is mapped to a token embedding in \mathbb{R}^K . Thus, token embeddings are represented as: $\mathbf{e}_i \in \mathbb{R}^K$, $\forall i \in \{1, 2, \dots, L\}$, where \mathbf{e}_i denotes the token embedding of the i -th nucleotide.

AggFirst In this approach, the embeddings are first aggregated, then passed through the learnable module Θ . In this approach, $NMD_{\text{efficiency}} = \Theta(\mathbf{A}(\{\mathbf{e}_i\}_{i=1}^L))$

AggLast Here, we first use a shared, learnable Θ to map each token embedding individually before aggregating them using \mathbf{A} . Therefore, $NMD_{\text{efficiency}} = \mathbf{A}(\{\Theta(\mathbf{e}_i)\}_{i=1}^L)$

DeepSet In the third approach, each token embedding is first passed through a shared, learnable submodule Φ to obtain a lower-dimensional representation. Next, the aggregation function \mathbf{A} is applied to combine the transformed embeddings into a single representation. Finally, another learnable submodule ρ is applied to the aggregated representation to predict NMD efficiency. This process can be formulated as: $NMD_{\text{efficiency}} = \rho(\mathbf{A}(\{\Phi(\mathbf{e}_i)\}_{i=1}^L))$

Baseline As a baseline, we trained a model with similar architecture and hyper-parameters using four binary features based on previous studies (Lindeboom et al., 2016; 2019): (1) **Last exon**: The stop-gain variant is located in the last exon of the transcript. (2) **Penultimate rule**: The nonsense variant occurs within the last 50 bp of the penultimate exon. (3) **Close to start**: The stop-gain variant is within 150 nucleotides of the start codon. (4) **Long exon**: The stop-gain variant is located in an exon longer than 407 bp.

Metrics During training, the model optimizes Mean Squared Error Loss (MSELoss). For evaluation, we compute five metrics: Mean Absolute Error (MAE), Root Mean Squared Error (RMSE), R^2 , Spearman correlation, and Pearson correlation.

Hyper-parameters and software For mRNA sequence extraction and processing, we used GenomeKit. Token embeddings were computed using Orthrus (Fradkin et al., 2024), a pretrained, Mamba-based mRNA foundation model. Model training was conducted in PyTorch (Paszke et al., 2019) with a learning rate of 5×10^{-4} and weight decay of 5×10^{-4} . The functions Θ , Φ , and ρ were implemented as multi-layer perceptrons (MLPs) with two hidden layers. Specifically, the hidden layers of Θ and Φ had a size of 8, while ρ had a hidden dimension of 4. To mitigate overfitting, we applied a dropout rate of 0.25 and trained the models for up to 50 epochs with early stopping.

2.3 NMDEP

We developed NMDEP by optimizing rule-based thresholds, curating potentially relevant features, and imputing features with high missingness, including half-life, mean ribosome-leading, and RNA location. Figure 3 provides an overview of the NMDEP workflow.

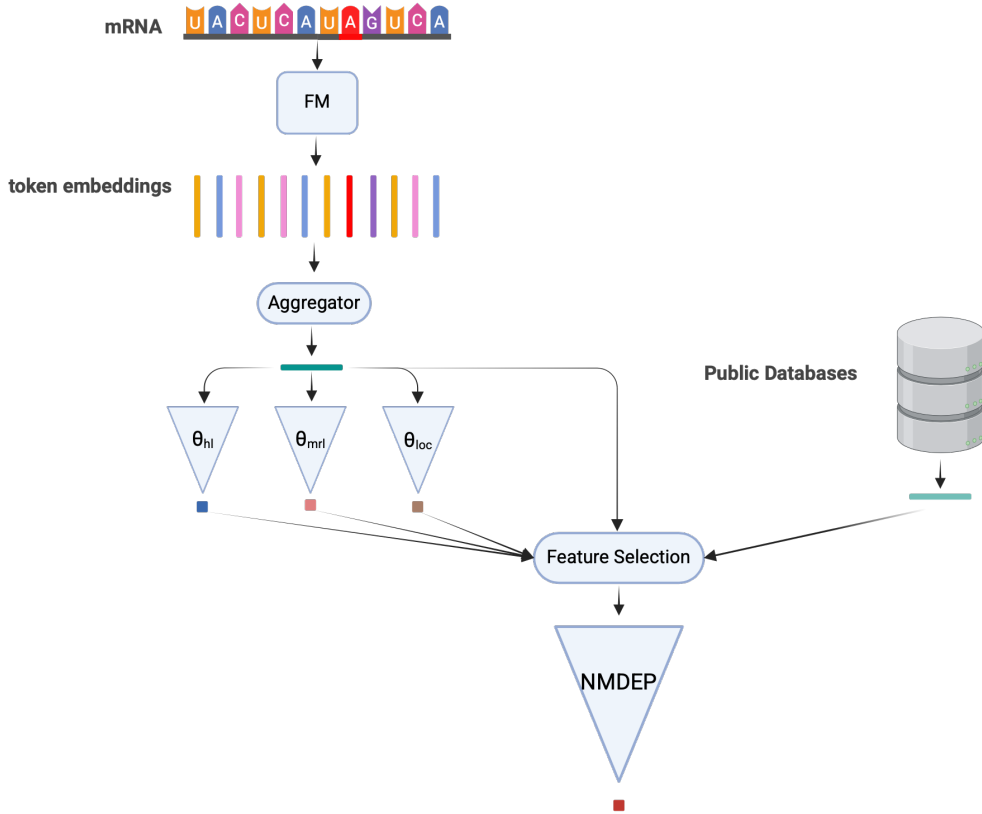


Figure 3: NMDEP development overview: mRNA sequences are processed through a foundation model (FM) to extract token embeddings, which are averaged and used to predict half-life, ribosome loading, and localization. The selected features are then fed into NMDEP, a two-layer MLP with a hidden size of 8 neurons. Figure created with BioRender.com

Feature threshold optimization Three of the four baseline features (penultimate rule, close to start, and long exon) rely on predefined thresholds. To determine the optimal values, we conducted a two-step grid search, selecting thresholds that minimized validation loss. In the first step, we explored a broad range of options. After identifying the values with the lowest validation loss, we refined the search by performing a second, more focused grid search around the selected thresholds. The final parameter ranges and step sizes are summarized in Table 1.

Feature annotation and selection For annotation, we extracted 76 potentially relevant features from public datasets, covering various aspects, including the position of the stop-gain variant, transcript and exon characteristics, evolutionary conservation and tolerance to variation, variant

Feature	First Grid Search	Second Grid Search
Penultimate exon	range = [25, 75], step = 5	range = [40, 50], step = 1
Start codon proximity	range = [50, 250], step = 25	range = [75, 125], step = 5
Exon length	range = [350, 450], step = 25	range = [350, 400], step = 5

Table 1: Grid search parameter ranges and step sizes for feature threshold optimization.

pathogenicity scores, intrinsic sequence properties, functional protein features, gene expression and regulation, and subcellular localization. Additionally, we incorporated the averaged mRNA Orthrus embeddings. For feature selection, we excluded features with low variance (< 0.01) or high correlation (> 0.8).

Auxiliary models Due to high missingness in three features including half-life (hl), mean ribosome loading (mrl), and subcellular localization we trained three auxiliary models to predict them using averaged Orthrus embeddings. This design is based on our benchmarking results (Table 2) which showed AggFirst approach with mean aggregator can perform well and is computationally efficient. Each auxiliary model is either an XGBoost regressor (for hl and mrl) or classifier (for localization), trained and tuned on 80% of the data using cross-validation and evaluated on the remaining 20%.

Model interpretation To interpret the model’s predictions, we used SHapley Additive exPlanations (SHAP) to assess global feature importance (Lundberg & Lee, 2017). SHAP quantifies each feature’s contribution by computing its average marginal impact across all possible feature combinations.

Genome-wide stop-gain variant simulation and NMDEP inference We used the Ensembl VariantSimulator to generate all possible single-nucleotide variants within coding regions. We then annotated these variants using VEP (McLaren et al., 2016) and retained only stop-gain variants in canonical transcripts. Finally, we applied NMDEP to estimate NMD efficiency for all retained variants.

3 RESULTS

3.1 BENCHMARKING SEQUENCE EMBEDDING REPRESENTATIONS

Table 2 summarizes the performance of the baseline model alongside three embedding-only approaches for NMD efficiency prediction. We observe that: 1) None of the embedding-only models outperform the baseline. 2) The choice of model, aggregation method, and sequence representation significantly affects performance. 3) Among the non-baseline approaches, using the mean aggregator for ALT sequence embeddings yields the best improvement. 4) DeepSet and AggLast offer performance gains but are computationally more demanding. 5) AggFirst, when combined with a mean aggregator and Alt sequence embeddings, achieves comparable performance while remaining computationally efficient.

3.2 NMDEP TRAINING, EVALUATION, AND APPLICATION

Feature optimization and selection We optimized the thresholds for three baseline features using a two-step grid search, both minimizing validation loss. The first search identified optimal thresholds over a broad range, while the second refined them around the best-performing values. The final thresholds are presented in Table 3, with Figures S1 and S2 depicting the search process.

Afterwards, we used these optimized features along with other potentially relevant feature (Table S1) and removed features with low variance or high correlation. This way we selected 60 features, as described in Table S2.

Auxiliary models performances The performance of the auxiliary models on the test set varied across tasks. For half-life prediction, the model achieved an MSE of 0.53, an MAE of 0.57, and a

Model	Aggregator	Sequence	MAE ↓	RMSE ↓	R^2 ↑	Spear. Corr ↑	Pear. Corr ↑
Baseline (4 rules)			0.8	1.07	0.35	0.67	0.6
AggFirst	mean	Alt	0.9	1.17	0.15	0.45	0.41
	max	Alt	1.09	1.33	0	NA	NA
	token	Alt	0.99	1.27	0.01	0.27	0.2
	sum	Alt	1.09	1.33	0	NA	NA
	mean	Alt - Ref	0.94	1.22	0.08	0.39	0.32
	max	Alt - Ref	1.06	1.31	0.03	0.24	0.2
	token	Alt - Ref	1.07	1.31	0.02	0.2	0.15
	sum	Alt - Ref	0.95	1.23	0.14	0.45	0.38
AggLast	mean	Alt	0.89	1.17	0.16	0.47	0.44
	max	Alt	0.94	1.28	0.06	0.46	0.45
	token	Alt	1.04	1.29	0.06	0.31	0.24
	sum	Alt	6.6	10.03	-60.95	0.08	0.04
	mean	Alt - Ref	0.93	1.18	0.14	0.42	0.39
	max	Alt - Ref	1.04	1.31	0.02	0.19	0.21
	token	Alt - Ref	1.03	1.30	0.04	0.24	0.21
	sum	Alt - Ref	2.83	3.4	-6.12	0.22	0.19
DeepSet	mean	Alt	0.89	1.16	0.18	0.47	0.45
	max	Alt	1	1.23	0.12	0.42	0.43
	token	Alt	1.06	1.31	0.02	0.19	0.13
	sum	Alt	1.1	1.45	-0.29	NA	NA
	mean	Alt - Ref	0.92	1.17	0.15	0.48	0.40
	max	Alt - Ref	1	1.3	0	0.19	0.14
	token	Alt - Ref	1.05	1.31	0.03	0.21	0.17
	sum	Alt - Ref	1.04	1.3	-0.04	0	-0.05

Table 2: Benchmarking of embedding-only methods for NMD efficiency prediction. NA: not available.

Feature	First Grid Search	Second Grid Search
Penultimate exon threshold	45.0	49.0
Start codon proximity threshold	100.0	120.0
Exon length threshold	375.0	355.0

Table 3: Optimized thresholds determined through a two-step grid search.

Spearman correlation of 0.68. For mean ribosome loading prediction, the model obtained an MSE of 0.61, an MAE of 0.63, and a Spearman correlation of 0.51. Finally, for subcellular localization classification, the model reached the accuracy of 0.70 and F1-score of 0.59.

NMDEP outperforms baseline and embedding-only models As shown in Table 4, NMDEP outperforms all other models, improving MAE by 10.7%, RMSE by 9.2%, R^2 by 24.4%, Spearman correlation by 7%, and Pearson correlation by 11%.

Model	MAE ↓	RMSE ↓	R^2 ↑	Spear. Corr ↑	Pear. Corr ↑
Baseline (4 rules)	0.8	1.07	0.35	0.67	0.6
4 rules optimized	0.75	0.98	0.41	0.71	0.66
Best of embedding-only models	0.89	1.16	0.18	0.48	0.45
Features from Kim et al. (2024)	0.78	1.06	0.3	0.63	0.56
NMDEP	0.67	0.89	0.51	0.76	0.73

Table 4: Performance comparison of models for NMD efficiency prediction.

NMDEP feature interpretation Figure 4 presents the top 15 features, demonstrating that NMDEP effectively leverages previously known factors (e.g., the last exon and penultimate rule) while also identifying potentially interesting features (e.g., mean ribosome loading). Additionally,

Figure 5 visualizes the SHAP values of all features across instances in the test set, providing evidence that each feature contributes meaningfully to the model's predictions.

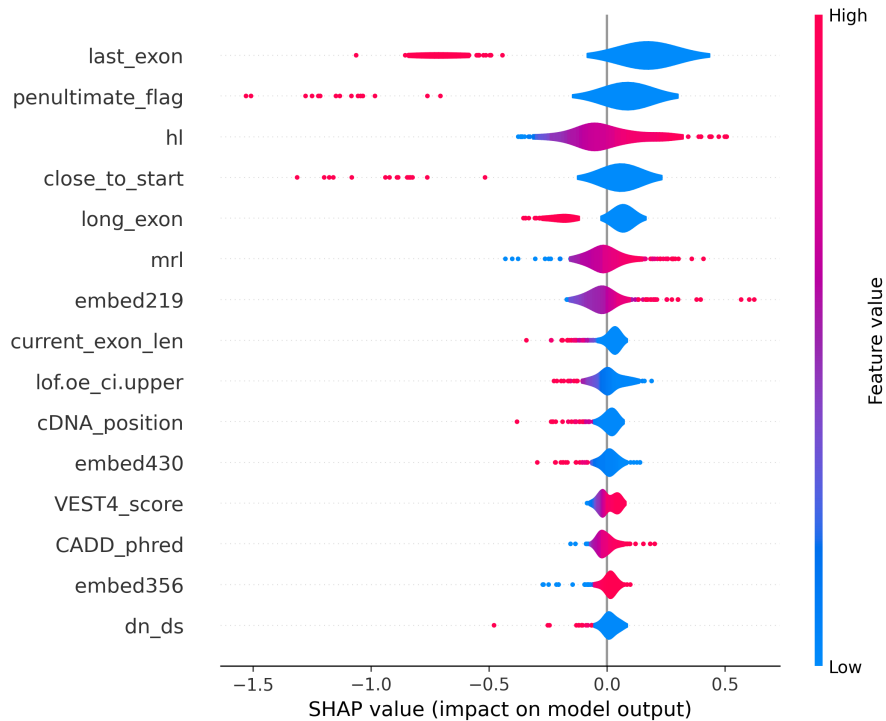


Figure 4: Top 15 important features for NMDEP, ranked by SHAP values, which indicate each feature's impact on the model output.

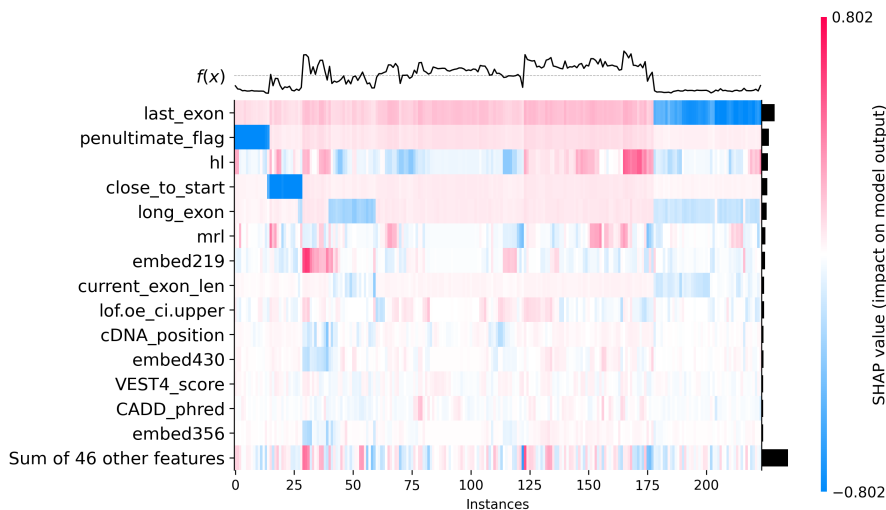


Figure 5: Heatmap of SHAP values for all test set samples. $f(x)$ is the model's output. Dark bars on the right indicate the overall contribution of each feature.

Genome-wide NMDEP inference We simulated 2,921,293 stop-gain variants across 18,372 unique transcripts and applied NMDEP to estimate their NMD efficiency. To demonstrate the utility of NMDEP, we present predictions for two genes.

First, *POLR3B*, a gene with many coding exons, exhibits variability in NMD efficiency across its sequence. Figure S3 illustrates these variations, while Figure S4 provides a heatmap for interpretation, highlighting that proximity to the start codon and in-silico pathogenicity score (CADD_{phred}) are the most influential factors.

Second, *TLR7*, which contains only a single coding exon, has consistently low NMD efficiency estimations, indicating that all stop-gain variants in this transcript can escape NMD (Figure S5). The SHAP value heatmap (Figure S6) reveals that conservation scores are the primary determinant of low NMD efficiency across *TLR7*.

4 DISCUSSION

We developed NMDEP, a machine learning framework that combines sequence embeddings with curated biological features to predict NMD efficiency, outperforming rule-based and embedding-only models. Our benchmarking analysis demonstrated that models relying solely on sequence embeddings underperformed compared to simple rule-based heuristics, underscoring the need for biologically informed feature integration. NMDEP overcomes the limitations of existing approaches and provides a more accurate, generalizable solution for NMD efficiency prediction.

Our analysis confirmed known determinants of NMD, such as variant position, while also identifying novel contributors, such as ribosome loading. Additionally, NMDEP's ability to predict NMD efficiency at single-variant resolution enabled a large-scale evaluation of more than 2.9 million simulated stop-gain variants, offering a systematic framework for assessing the impact of premature stop codons on transcript stability.

Despite its strong performance, NMDEP does not account for tissue-specific variations, which may limit its applicability across diverse biological contexts (Palou-Marquez & Supek, 2024). Additionally, NMDEP may not fully capture the diverse regulatory mechanisms governing NMD.

Future work will enhance NMDEP by integrating tissue-specific NMD data for more precise predictions and incorporating frameshift and splicing effects to improve transcript stability modeling (Litchfield et al., 2020; McGlincy & Smith, 2008). Additionally, exploring its clinical utility in prioritizing pathogenic stop-gain variants will help translate predictions into real-world applications, advancing transcriptome regulation and disease understanding.

REFERENCES

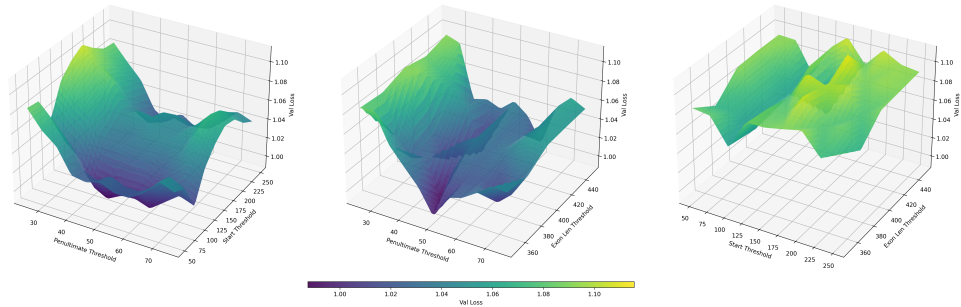
- Vikram Agarwal and David R Kelley. The genetic and biochemical determinants of mRNA degradation rates in mammals. *Genome Biol.*, 23(1):245, November 2022.
- Cancer Genome Atlas Research Network, John N Weinstein, Eric A Collisson, Gordon B Mills, Kenna R Mills Shaw, Brad A Ozenberger, Kyle Ellrott, Ilya Shmulevich, Chris Sander, and Joshua M Stuart. The cancer genome atlas Pan-Cancer analysis project. *Nat. Genet.*, 45(10):1113–1120, October 2013.
- Hannah Carter, Christopher Douville, Peter D Stenson, David N Cooper, and Rachel Karchin. Identifying mendelian disease genes with the variant effect scoring tool. *BMC Genomics*, 14 Suppl 3 (S3):S3, May 2013.
- Yao-Fu Chang, J Saadi Imam, and Miles F Wilkinson. The nonsense-mediated decay RNA surveillance pathway. *Annu. Rev. Biochem.*, 76(1):51–74, June 2007.
- Zeynep Coban-Akdemir, Janson J White, Xiaofei Song, Shalini N Jhangiani, Jawid M Fatih, Tomasz Gambin, Yavuz Bayram, Ivan K Chinn, Ender Karaca, Jaya Punetha, Cecilia Poli, Eric Boerwinkle, Chad A Shaw, Jordan S Orange, Richard A Gibbs, Tuuli Lappalainen, James R Lupski, and Claudia M B Carvalho. Identifying genes whose mutant transcripts cause dominant disease traits by potential gain-of-function alleles. *Am. J. Hum. Genet.*, 103(2):171–187, August 2018.
- Tianyu Cui, Yiyang Dou, Puwen Tan, Zhen Ni, Tianyuan Liu, Duolin Wang, Yan Huang, Kaican Cai, Xiaoyang Zhao, Dong Xu, Hao Lin, and Dong Wang. RNALocate v2.0: an updated resource for RNA subcellular localization with increased coverage and annotation. *Nucleic Acids Res.*, 50 (D1):D333–D339, January 2022.

- Philip Fradkin, Ruian Shi, Keren Isaev, Brendan J Frey, Quaid Morris, Leo J Lee, and Bo Wang. Orthrus: Towards evolutionary and functional RNA foundation models. December 2024.
- Deep Genomics GenomeKit. URL <https://github.com/deepgenomics/GenomeKit>.
- Daniel C Jeffares, Bartłomiej Tomiczek, Victor Sojo, and Mario dos Reis. A beginners guide to estimating the non-synonymous to synonymous rate ratio of all protein-coding genes in a genome. *Methods Mol. Biol.*, 1201:65–90, 2015.
- Konrad J Karczewski, Laurent C Francioli, Grace Tiao, Beryl B Cummings, Jessica Alföldi, Qingbo Wang, Ryan L Collins, Kristen M Laricchia, Andrea Ganna, Daniel P Birnbaum, Laura D Gauthier, Harrison Brand, Matthew Solomonson, Nicholas A Watts, Daniel Rhodes, Moriel Singer-Berk, Eleina M England, Eleanor G Seaby, Jack A Kosmicki, Raymond K Walters, Katherine Tashman, Yossi Farjoun, Eric Banks, Timothy Poterba, Arcturus Wang, Cotton Seed, Nicola Whiffin, Jessica X Chong, Kaitlin E Samocha, Emma Pierce-Hoffman, Zachary Zappala, Anne H O’Donnell-Luria, Eric Vallabh Minikel, Ben Weisburd, Monkol Lek, James S Ware, Christopher Vittal, Irina M Armean, Louis Bergelson, Kristian Cibulskis, Kristen M Connolly, Miguel Covarubias, Stacey Donnelly, Steven Ferriera, Stacey Gabriel, Jeff Gentry, Namrata Gupta, Thibault Jeandet, Diane Kaplan, Christopher Llanwarne, Ruchi Munshi, Sam Novod, Nikelle Petrillo, David Roazen, Valentin Ruano-Rubio, Andrea Saltzman, Molly Schleicher, Jose Soto, Kathleen Tibbetts, Charlotte Tolonen, Gordon Wade, Michael E Talkowski, Genome Aggregation Database Consortium, Benjamin M Neale, Mark J Daly, and Daniel G MacArthur. The mutational constraint spectrum quantified from variation in 141,456 humans. *Nature*, 581(7809):434–443, May 2020.
- Young-Gon Kim, Hyunju Kang, Beomki Lee, Hyeok-Jae Jang, Jong-Ho Park, Changhee Ha, Hogun Park, and Jong-Won Kim. A spectrum of nonsense-mediated mRNA decay efficiency along the degree of mutational constraint. *Commun. Biol.*, 7(1):1461, November 2024.
- Jonathan Klonowski, Qianqian Liang, Zeynep Coban-Akdemir, Cecilia Lo, and Dennis Kostka. Aenmd: Annotating escape from nonsense-mediated decay for transcripts with protein-truncating variants. *Bioinformatics*, 39(9), September 2023.
- Tatsuaki Kurosaki, Maximilian W Popp, and Lynne E Maquat. Quality and quantity control of gene expression by nonsense-mediated mRNA decay. *Nat. Rev. Mol. Cell Biol.*, 20(7):406–420, July 2019.
- Rik G H Lindeboom, Fran Supek, and Ben Lehner. The rules and impact of nonsense-mediated mRNA decay in human cancers. *Nat. Genet.*, 48(10):1112–1118, October 2016.
- Rik G H Lindeboom, Michiel Vermeulen, Ben Lehner, and Fran Supek. The impact of nonsense-mediated mRNA decay on genetic disease, gene editing and cancer immunotherapy. *Nat. Genet.*, 51(11):1645–1651, November 2019.
- Kevin Litchfield, James L Reading, Emilia L Lim, Hang Xu, Po Liu, Maise Al-Bakir, Yien Ning Sophia Wong, Andrew Rowan, Samuel A Funt, Taha Merghoub, David Perkins, Martin Lauss, Inge Marie Svane, Göran Jönsson, Javier Herrero, James Larkin, Sergio A Quezada, Matthew D Hellmann, Samra Turajlic, and Charles Swanton. Escape from nonsense-mediated decay associates with anti-tumor immunogenicity. *Nat. Commun.*, 11(1):3800, July 2020.
- Scott M Lundberg and Su-In Lee. A unified approach to interpreting model predictions. In I. Guyon, U. V. Luxburg, S. Bengio, H. Wallach, R. Fergus, S. Vishwanathan, and R. Garnett (eds.), *Advances in Neural Information Processing Systems 30*, pp. 4765–4774. Curran Associates, Inc., 2017. URL <http://papers.nips.cc/paper/7062-a-unified-approach-to-interpreting-model-predictions.pdf>.
- Nicholas J McGlincy and Christopher W J Smith. Alternative splicing resulting in nonsense-mediated mRNA decay: what is the meaning of nonsense? *Trends Biochem. Sci.*, 33(8):385–393, August 2008.
- William McLaren, Laurent Gil, Sarah E Hunt, Harpreet Singh Riat, Graham R S Ritchie, Anja Thormann, Paul Flicek, and Fiona Cunningham. The ensembl variant effect predictor. *Genome Biol.*, 17(1), December 2016.

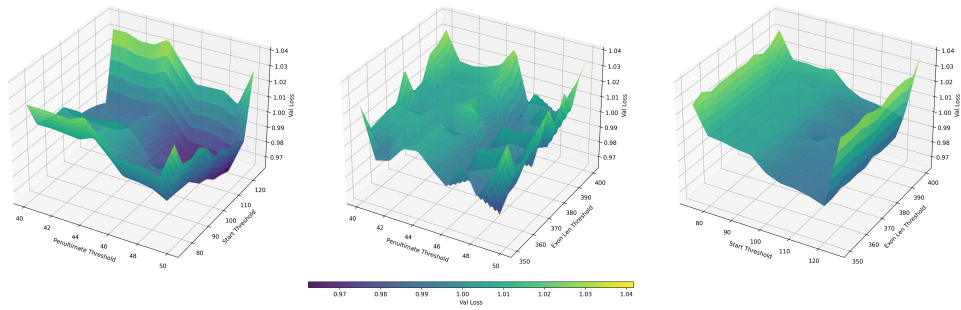
- Guillermo Palou-Marquez and Fran Supek. Variable efficiency of nonsense-mediated mRNA decay across human tissues, tumors and individuals. March 2024.
- Adam Paszke, Sam Gross, Francisco Massa, Adam Lerer, James Bradbury, Gregory Chanan, Trevor Killeen, Zeming Lin, Natalia Gimelshein, Luca Antiga, Alban Desmaison, Andreas Köpf, Edward Yang, Zach DeVito, Martin Raison, Alykhan Tejani, Sasank Chilamkurthy, Benoit Steiner, Lu Fang, Junjie Bai, and Soumith Chintala. PyTorch: An imperative style, high-performance deep learning library. 2019.
- Katherine S Pollard, Melissa J Hubisz, Kate R Rosenbloom, and Adam Siepel. Detection of nonneutral substitution rates on mammalian phylogenies. *Genome Res.*, 20(1):110–121, January 2010.
- Philipp Rentzsch, Daniela Witten, Gregory M Cooper, Jay Shendure, and Martin Kircher. CADD: predicting the deleteriousness of variants throughout the human genome. *Nucleic Acids Res.*, 47(D1):D886–D894, January 2019.
- Manuel A Rivas, Matti Pirinen, Donald F Conrad, Monkol Lek, Emily K Tsang, Konrad J Karczewski, Julian B Maller, Kimberly R Kukurba, David S DeLuca, Menachem Fromer, Pedro G Ferreira, Kevin S Smith, Rui Zhang, Fengmei Zhao, Eric Banks, Ryan Poplin, Douglas M Ruderfer, Shaun M Purcell, Taru Tukiainen, Eric V Minikel, Peter D Stenson, David N Cooper, Katharine H Huang, Timothy J Sullivan, Jared Nedzel, GTEx Consortium, Geuvadis Consortium, Carlos D Bustamante, Jin Billy Li, Mark J Daly, Roderic Guigo, Peter Donnelly, Kristin Ardlie, Michael Sammeth, Emmanouil T Dermitzakis, Mark I McCarthy, Stephen B Montgomery, Tuuli Lappalainen, and Daniel G MacArthur. Human genomics. effect of predicted protein-truncating genetic variants on the human transcriptome. *Science*, 348(6235):666–669, May 2015.
- Mark F Rogers, Hashem A Shihab, Matthew Mort, David N Cooper, Tom R Gaunt, and Colin Campbell. FATHMM-XF: accurate prediction of pathogenic point mutations via extended features. *Bioinformatics*, 34(3):511–513, February 2018.
- Ali Saadat and Jacques Fellay. Fine-tuning the ESM2 protein language model to understand the functional impact of missense variants. 2024.
- Yoichiro Sugimoto and Peter J Ratcliffe. Isoform-resolved mRNA profiling of ribosome load defines interplay of HIF and mTOR dysregulation in kidney cancer. *Nat. Struct. Mol. Biol.*, 29(9):871–880, September 2022.
- Fran Supek, Ben Lehner, and Rik G H Lindeboom. To NMD or not to NMD: Nonsense-mediated mRNA decay in cancer and other genetic diseases. *Trends Genet.*, 37(7):657–668, July 2021.
- Nicole A Teran, Daniel C Nachun, Tiffany Eulalio, Nicole M Ferraro, Craig Smail, Manuel A Rivas, and Stephen B Montgomery. Nonsense-mediated decay is highly stable across individuals and tissues. *Am. J. Hum. Genet.*, 108(8):1401–1408, August 2021.
- Rebecca I Torene, Maria J Guillen Sacoto, Francisca Millan, Zhancheng Zhang, Stephen McGee, Matthew Oetjens, Elizabeth Heise, Karen Chong, Richard Sidlow, Lauren O’Grady, Inderneel Sahai, Christa L Martin, David H Ledbetter, Scott M Myers, Kevin J Mitchell, and Kyle Retterer. Systematic analysis of variants escaping nonsense-mediated decay uncovers candidate mendelian diseases. *Am. J. Hum. Genet.*, 111(1):70–81, January 2024.
- Ensembl VariantSimulator. URL <https://www.ensembl.org/info/docs/tools/simulator/index.html>.
- Manzil Zaheer, Satwik Kottur, Siamak Ravanbakhsh, Barnabas Poczos, Ruslan Salakhutdinov, and Alexander Smola. Deep sets. 2017.
- Tony Zeng, Jeffrey P Spence, Hakhamanesh Mostafavi, and Jonathan K Pritchard. Bayesian estimation of gene constraint from an evolutionary model with gene features. *Nat. Genet.*, 56(8):1632–1643, August 2024.

A APPENDIX

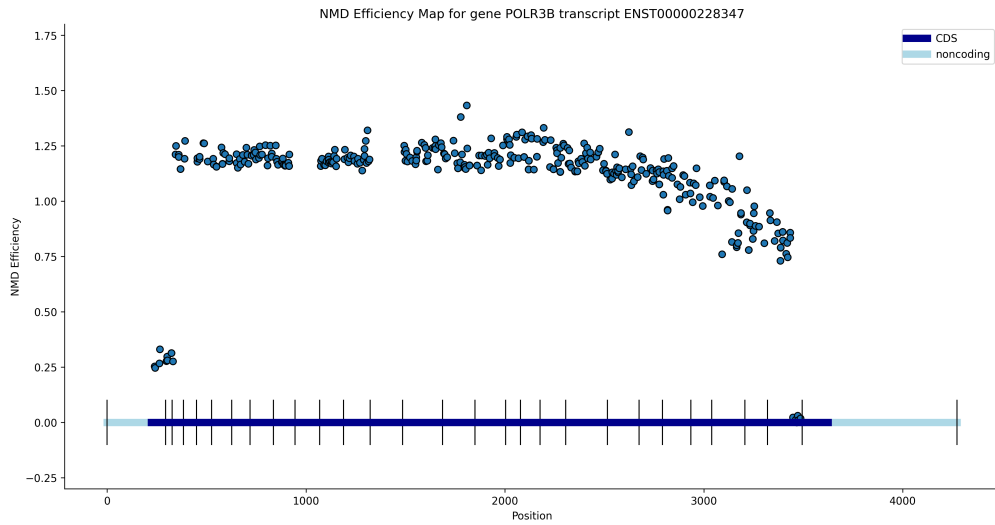
A.1 SUPPLEMENTARY FIGURES



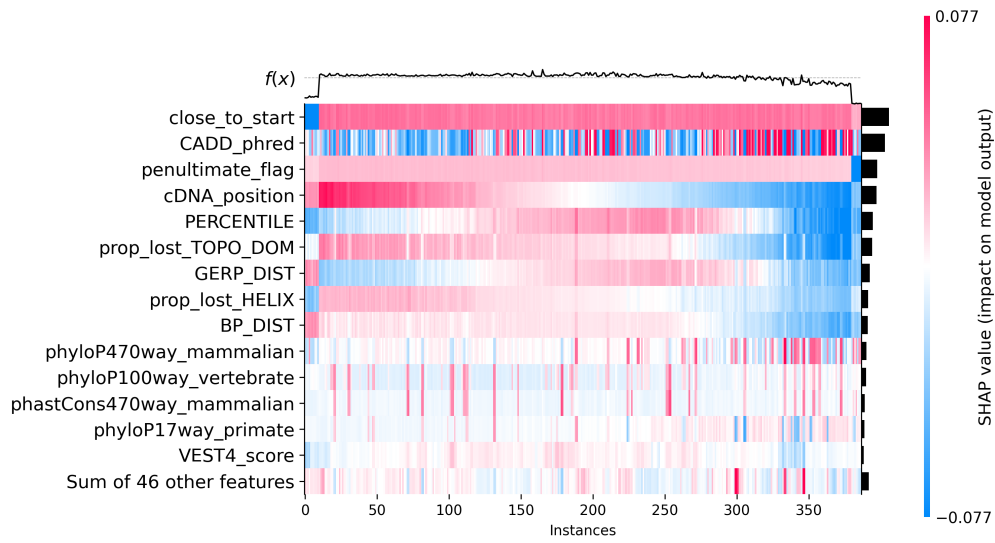
Supplementary Figure S1: First grid search results: Optimization of validation loss by varying thresholds.



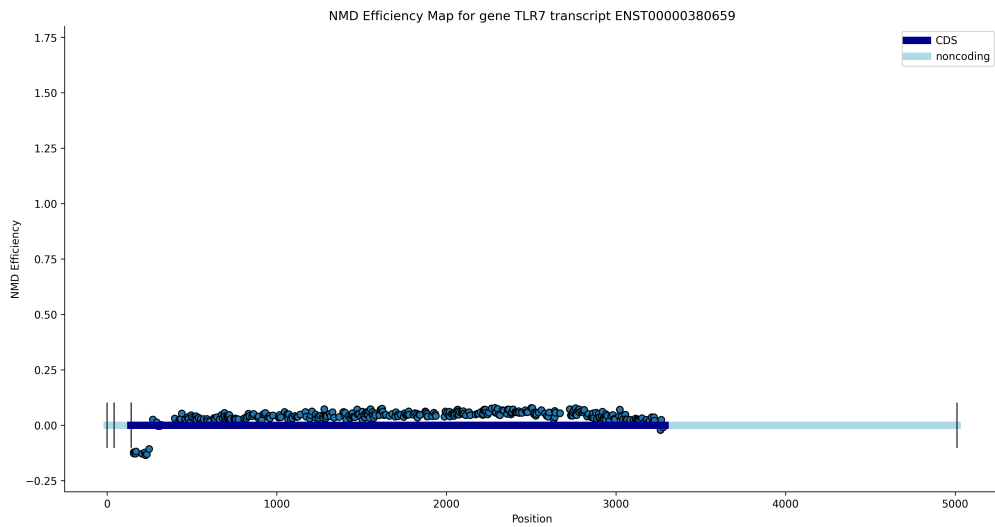
Supplementary Figure S2: Second grid search results: Refinement of validation loss optimization by adjusting thresholds based on the first grid search results.



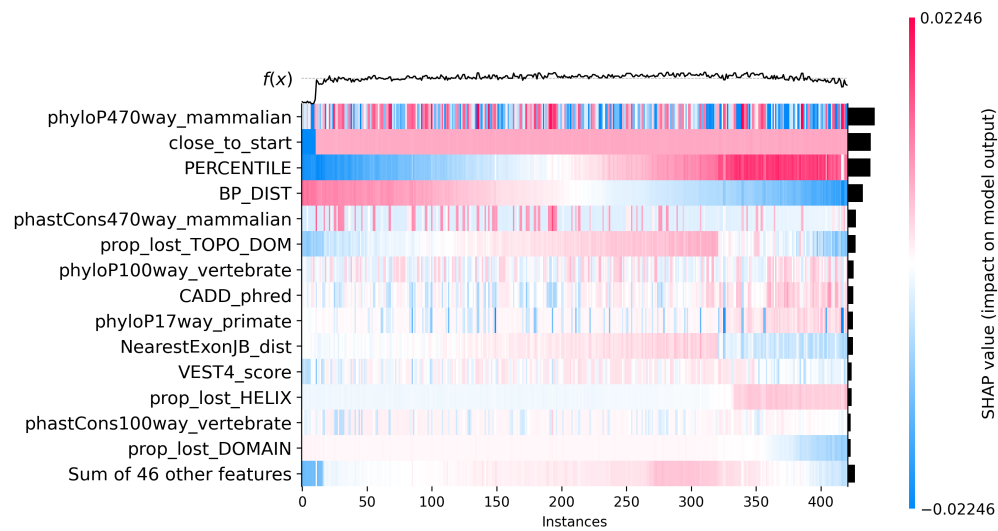
Supplementary Figure S3: NMDEP estimations for all simulated stop-gain variants across *POLR3B*. Vertical lines indicate exon boundaries.



Supplementary Figure S4: Heatmap of SHAP values for all simulated stop-gain variants across *POLR3B*. $f(x)$ is the model's output. Dark bars on the right indicate the overall contribution of each feature.



Supplementary Figure S5: NMDEP estimations for all simulated stop-gain variants across *TLR7*. Vertical lines indicate exon boundaries.



Supplementary Figure S6: Heatmap of SHAP values for all simulated stop-gain variants across *TLR7*. $f(x)$ is the model's output. Dark bars on the right indicate the overall contribution of each feature.

A.2 SUPPLEMENTARY TABLES

Feature	Description
cDNA_position (McLaren et al., 2016)	Position of the mutation within the cDNA sequence.
CDS_position (McLaren et al., 2016)	Position of the mutation within the coding sequence.
Protein_position (McLaren et al., 2016)	Position of the mutation in the translated protein.
PERCENTILE (Karczewski et al., 2020)	Percentile of the mutation's position.
BP_DIST (Karczewski et al., 2020)	Nucleotide distance from the variant position to the stop codon
GERP_DIST (Karczewski et al., 2020)	GERP-weighted distance from a variant position.
last_exon	Indicates if the mutation occurs in the last exon.
long_exon	Whether the affected exon is considered long.
penultimate_flag	Whether the mutation is in the last 49bp of second-to-last exon.
single_exon	Whether the gene has a single exon.
current_exon_number (McLaren et al., 2016)	Exon number where the mutation is located.
total_exon_numbers (McLaren et al., 2016)	Total number of exons in the gene.
DIST_FROM_LAST_EXON (Karczewski et al., 2020)	Distance of the mutation from the last exon.
NearestExonJB_dist (McLaren et al., 2016)	Distance to the nearest exon junction boundary.
close_to_start	Whether the mutation is near the start codon.
utr5_len (GenomeKit)	Length of the 5' UTR.
utr3_len (GenomeKit)	Length of the 3' UTR.
total_cds_len (GenomeKit)	Total length of the coding sequence.
total_exons_len (GenomeKit)	Total length of all exons in the gene.
current_exon_len (GenomeKit)	Length of the exon where the mutation occurs.
hl (Agarwal & Kelley, 2022)	Estimated half-life of the mRNA.
mrl (Sugimoto & Ratcliffe, 2022)	mean ribosome load.
phyloP100way_vertebrate (Pollard et al., 2010)	Phylogenetic conservation across 100 vertebrate species.
phyloP17way_primate (Pollard et al., 2010)	Phylogenetic conservation across 17 primates.
phyloP470way_mammalian (Pollard et al., 2010)	Phylogenetic conservation across 470 mammals.
phastCons100way_vertebrate (Pollard et al., 2010)	Conservation score across 100 vertebrates.
phastCons17way_primate (Pollard et al., 2010)	Conservation score across 17 primates.
phastCons470way_mammalian (Pollard et al., 2010)	Conservation score across 470 mammals.
dn_ds (Jeffares et al., 2015)	Ratio of nonsynonymous to synonymous mutations.
lof.pLI (Karczewski et al., 2020)	Probability of being loss-of-function intolerant.
lof.pRec (Karczewski et al., 2020)	Probability of intolerance to homozygous mutations.
lof.pNull (Karczewski et al., 2020)	Probability of being tolerant to LoF variants.
mis.z_score (Karczewski et al., 2020)	Z-score for missense constraint.
syn.z_score (Karczewski et al., 2020)	Z-score for synonymous constraint.
lof.oe.ci.upper(Karczewski et al., 2020)	Upper bound of observed/expected LoF variation confidence interval.
VEST4_score (Carter et al., 2013)	VEST4 pathogenicity predictor.
CADD.phred (Rentzsch et al., 2019)	CADD pathogenicity predictor.
fathmm-XF_coding_score (Rogers et al., 2018)	fathmm-XF pathogenicity predictor.
LoF_HC (Karczewski et al., 2020)	High-confidence loss-of-function (based on LOFTEE).
gnomad41_genome_AF (Karczewski et al., 2020)	Allele frequency in the gnomAD genome dataset.
gnomad41_exome_AF (Karczewski et al., 2020)	Allele frequency in the gnomAD exome dataset.
CDS_GC (GenomeKit)	GC content of the coding sequence.
UTR3_GC (GenomeKit)	GC content of the 3' UTR.
UTR5_GC (GenomeKit)	GC content of the 5' UTR.
embedX (Fradkin et al., 2024)	Sequence embedding generated using Orthrus. X is between 0 to 51
prop_lost_ACT_SITE (Saadat & Fellay, 2024)	Proportion of active site lost due to mutation.
prop_lost_BINDING (Saadat & Fellay, 2024)	Proportion of binding sites lost.
prop_lost_COILED (Saadat & Fellay, 2024)	Proportion of coiled-coil regions lost.
prop_lost_COMPBIAS (Saadat & Fellay, 2024)	Proportion of compositionally biased regions lost.
prop_lost_DISULFID (Saadat & Fellay, 2024)	Proportion of disulfide bonds lost.
prop_lost_DOMAIN (Saadat & Fellay, 2024)	Proportion of functional domains lost.
prop_lost_HELIX (Saadat & Fellay, 2024)	Proportion of alpha-helices lost.
prop_lost_MOD_RES (Saadat & Fellay, 2024)	Proportion of modified residues lost.
prop_lost_MOTIF (Saadat & Fellay, 2024)	Proportion of sequence motifs lost.
prop_lost_PROPEP (Saadat & Fellay, 2024)	Proportion of propeptide regions lost.

Feature	Description
prop_lost_REGION (Saadat & Fellay, 2024)	Proportion of functionally relevant regions lost.
prop_lost_REPEAT (Saadat & Fellay, 2024)	Proportion of repeat regions lost.
prop_lost_SIGNAL (Saadat & Fellay, 2024)	Proportion of signal peptides lost.
prop_lost_STRAND (Saadat & Fellay, 2024)	Proportion of beta-strands lost.
prop_lost_TOPO_DOM (Saadat & Fellay, 2024)	Proportion of topological domains lost.
prop_lost_TRANSIT (Saadat & Fellay, 2024)	Proportion of transit peptides lost.
prop_lost_TRANSMEM (Saadat & Fellay, 2024)	Proportion of transmembrane regions lost.
prop_lost_TURN (Saadat & Fellay, 2024)	Proportion of beta-turns lost.
prop_lost_ZN_FING (Saadat & Fellay, 2024)	Proportion of zinc finger domains lost.
abundance (Zeng et al., 2024)	abundance level.
exp_var (Zeng et al., 2024)	Variability of RNA expression across tissues.
tau (Zeng et al., 2024)	Tissue specificity of gene expression.
connectedness (Zeng et al., 2024)	Connectivity of the gene in coexpression networks.
betweenness (Zeng et al., 2024)	Centrality of the gene in protein-protein interaction networks.
TF (Zeng et al., 2024)	Whether the gene encodes a transcription factor.
Nucleus (Cui et al., 2022)	localization in the nucleus.
Exosome (Cui et al., 2022)	localization in exosomes.
Cytosol (Cui et al., 2022)	localization in the cytosol.
Cytoplasm (Cui et al., 2022)	localization in the cytoplasm.
Ribosome (Cui et al., 2022)	localization in ribosomes.
Membrane (Cui et al., 2022)	localization is membrane-bound.
Endoplasmic_reticulum (Cui et al., 2022)	localization in the endoplasmic reticulum.

Supplementary Table S1: List of initially annotated features.

Feature	Category	Description
last_exon	Transcript and Exon Features	Indicates if the mutation occurs in the last exon.
long_exon	Transcript and Exon Features	Whether the affected exon is considered long.
penultimate_flag	Transcript and Exon Features	Whether the mutation is in the last 49bp of second-to-last exon.
close_to_start	Transcript and Exon Features	Whether the mutation is near the start codon.
hl	Transcript and Exon Features	Estimated half-life of the mRNA.
mrl	Transcript and Exon Features	Mean ribosome load.
cDNA_position	Position of Stop-Gain Variant	Position of the mutation within the cDNA sequence.
PERCENTILE	Position of Stop-Gain Variant	Percentile of the mutation's position.
GERP_DIST	Position of Stop-Gain Variant	GERP-weighted distance from a variant position.
BP_DIST	Position of Stop-Gain Variant	Nucleotide distance from the variant position to the stop codon.
utr5_len	Transcript and Exon Features	Length of the 5' UTR.
current_exon_len	Transcript and Exon Features	Length of the exon where the mutation occurs.
VEST4_score	Variation Pathogenicity	VEST4 pathogenicity predictor.
CADD_phred	Variation Pathogenicity	CADD pathogenicity predictor.
phyloP100way Vertebrate	Conservation and Tolerance	Phylogenetic conservation across 100 vertebrate species.
dn_ds	Conservation and Tolerance	Ratio of nonsynonymous to synonymous mutations.
abundance	Expression and Regulation	Abundance level.
shet	Conservation and Tolerance	Posterior mean for shet.
lof.oe.ci.upper	Conservation and Tolerance	Upper bound of observed/expected LoF variation confidence.
lof.pRec	Conservation and Tolerance	Probability of intolerance to homozygous mutations.
UTR5_GC	Intrinsic Sequence Features	GC content of the 5' UTR.
connectedness	Expression and Regulation	Connectivity of the gene in coexpression networks.
prop_lost_DOMAIN	Functional Protein Features	Proportion of functional domains lost.
prop_lost_HELIX	Functional Protein Features	Proportion of alpha-helices lost.
prop_lost_REGION	Functional Protein Features	Proportion of functionally relevant regions lost.
prop_lost_TOPO_DOM	Functional Protein Features	Proportion of topological domains lost.
LoF_HC	Variation Pathogenicity	High-confidence loss-of-function (based on LOFTEE).
NearestExonJB_dist	Transcript and Exon Features	Distance to the nearest exon junction boundary.
TF	Expression and Regulation	Whether the gene encodes a transcription factor.
tau	Expression and Regulation	Tissue specificity of gene expression.
phyloP17way primate	Conservation and Tolerance	Phylogenetic conservation across 17 primates.

Feature	Category	Description
phyloP470way_mammalian	Conservation and Tolerance	Phylogenetic conservation across 470 mammals.
phastCons100way Vertebrate	Conservation and Tolerance	Conservation score across 100 vertebrates.
phastCons17way_primate	Conservation and Tolerance	Conservation score across 17 primates.
phastCons470way_mammalian	Conservation and Tolerance	Conservation score across 470 mammals.
mis.z_score	Conservation and Tolerance	Z-score for missense constraint.
syn.z_score	Conservation and Tolerance	Z-score for synonymous constraint.
lof.pNull	Conservation and Tolerance	Probability of being tolerant to LoF variants.
exp_var	Expression and Regulation	Variability of RNA expression across tissues.
utr3_len	Transcript and Exon Features	Length of the 3' UTR.
total_exons_len	Transcript and Exon Features	Total length of all exons in the gene.
fathmm-XF_coding_score	Variant Pathogenicity	fathmm-XF pathogenicity predictor.
Nucleus	Subcellular Localization	Localization in the nucleus.
Cytosol	Subcellular Localization	Localization in the cytosol.
Cytoplasm	Subcellular Localization	Localization in the cytoplasm.
Ribosome	Subcellular Localization	Localization in ribosomes.
Membrane	Subcellular Localization	Localization is membrane-bound.
Endoplasmic_reticulum	Subcellular Localization	Localization in the endoplasmic reticulum.
embed6	Intrinsic Sequence Features	Sequence embedding 6 from Orthrus.
embed8	Intrinsic Sequence Features	Sequence embedding 8 from Orthrus.
embed90	Intrinsic Sequence Features	Sequence embedding 90 from Orthrus.
embed145	Intrinsic Sequence Features	Sequence embedding 145 from Orthrus.
embed205	Intrinsic Sequence Features	Sequence embedding 205 from Orthrus.
embed219	Intrinsic Sequence Features	Sequence embedding 219 from Orthrus.
embed230	Intrinsic Sequence Features	Sequence embedding 230 from Orthrus.
embed240	Intrinsic Sequence Features	Sequence embedding 240 from Orthrus.
embed254	Intrinsic Sequence Features	Sequence embedding 254 from Orthrus.
embed309	Intrinsic Sequence Features	Sequence embedding 309 from Orthrus.
embed356	Intrinsic Sequence Features	Sequence embedding 356 from Orthrus.
embed430	Intrinsic Sequence Features	Sequence embedding 430 from Orthrus.

Supplementary Table S2: List of selected features and their descriptions.